Symmetry Conservation of Dirac Fermion With Double Junction and Gauge Field of Weyl Fermion With Single Junction

Teresa Oh (teresa@cju.ac.kr)
Cheongju University
Xiangjiang Li
School of Information Engineering, Nanyang Institute of Technology
Jing Fan
School of Information Engineering, Nanyang Institute of Technology

Research Article

Keywords: Phase isolator, Electron polarization, Dirac insulator, Majorana fermion, Spin current

Posted Date: December 11th, 2020

DOI: https://doi.org/10.21203/rs.3.rs-122122/v1

Symmetry conservation of Dirac fermion with double junction and gauge field of Weyl fermion with single junction

Teresa Oh[1*], Xiangjiang Li[2], Jing Fan[2,]

[1]Department of Semiconductor Engineering, Cheongju University, Cheongju 28503, Republic of Korea

[2]School of Information Engineering, Nanyang Institute of Technology, Nanyang 473004, China

Keywords: Phase isolator; Electron polarization; Dirac insulator; Majorana fermion; Spin current;

*Corresponding author : teresa@cju.ac.kr

Abstract

Majorana fermion and Weyl fermion have matters and antimatters. But Majorana fermion has zero resistance and Weyl fermion has a resistance. It was confirmed that CP symmetry is preserved in the case of Dirac fermion because it only has spin current as the antimatter. Dirac fermion is supercurrent because CP symmetry is preserved by double schottky contact, but the Majorana fermion with ohmic contact has decreased current due to symmetry violation. Parity symmetry conservation was confirmed from the electrical properties of transistors, and charge symmetry conservation was confirmed in diode properties.

1. Introduction

The study of superconductors operating on the basis of magnetic energy is mainly dealt with in the field of spintronics and is classified as a two-class superconductor. The study of superconductors began in 1911 when mercury was observed to be resistance zero by the Onnes of the Netherlands, and the principle of operation of superconductors was found to be BCS theory. In 1957, the BCS theory explained the superconductor theoretically with two pairs of electronic coopers consisting of reverse spin direction. In order to confirm superconductivity, the resistance must be demonstrated to be zero, to prevent the moving of electrons and to appear the moving of spins, Meissner effect (resistance R=0) occurs in a strong magnetic field and at very low temperatures[1-2]. In superconductors, there are many materials that have emerged as semiconductor technology has developed. The theory of copper-based semi-conductors in 1987 and iron-based superconductors in 2006 is described as spin-density wave (SDW). A superconductor that has been studied recently is a phase insulator. Phase insulators are internal insulators, but surface currents flow from the surface. To become a topological insulator, a small, thin 2D structure and magnetic field and low temperature are required[3-5].

By using semiconductor-specific process technology, it can be made from a large area of material. The same material also increases its energy electromagnetic as its surface area widens. Thus, the topological insulator has superconductivity without magnetic field due to its structural effect with a large area.

Therefore, topological insulators have high surface energy, so the electronic energy relationships and differences of common insulators appear. Typically, topological insulators exhibit superconductivity without a magnetic field. This is called the Anomalous Quantum Hall Effect (AQHE). The surface current of the phase insulator starts from the kinetic energy of the spin rotation by the kinetic momentum of the electron. The magnetic field is generated by the electro-momentum and spin motion, and magnetic energy forms a spin current[6-8].

The electron and spin are related to the matter and the antimatter. The electron, which is the matter, makes the charge current, and the spin, which is the antimatter, makes the spin current[9-12]. Matters and antimatters have the same physical quantity physically and chemically, but have a relationship of chiral symmetry, with opposite polarity electrically. Therefore, the charge current and spin current are opposite in polarity. The charge current has a + resistance in the field, and the spin current shows a negative resistance in the magnetic field. The spin current of the topological insulator is negative resistance characteristic and there is no loss of thermal resistance, so the super current flows[13-16]. Thus the topological insulator is an insulator, but it is the principle of current flow. Studies of insulators have led to studies of schottky contact and low-k materials[17-19], and recently reported that low-k materials are phase insulators[3].

There has been a lot of research in the past on the cause of the increase in current values due to schottky contact. Schottky contact is caused by a depletion layer that occurs in the interface of semiconductor PN junction, and it is a good environment for schottky contact to make spin current, so it is highly likely that super current will be created[20-21]. Schottky resistance by schottky contact is the opposite concept of ohmic resistance. Low-k material produces spin current from a material that implements a schottky contact, so low-k makes it 10 times faster than normal OTFT movement[22]. Electromagnetic energy is preserved by Lenz's law. Matters and antimatters are

symmetrical, and the antimatter of electrons are spin. The causes of the spin current of Majorana fermion,[23] Dirac fermion and Weyl fermion start from the electromagnetic energy momentum and the gauge field will occur when the energy gap is separated. Understanding the relationship between electromagnetic energy momentum and gauge field helps to understand the state of spin, quantum-spin-hole effect and abnormal quantum hall effect. Unusual phenomena and studies of phase insulators are being reported as they create spin currents.[24-26]
The conservation of the symmetry of fermion from the electrical properties of transistors using phase insulator was studied.

2. Symmetry violation of Majorana fermion and gauge field

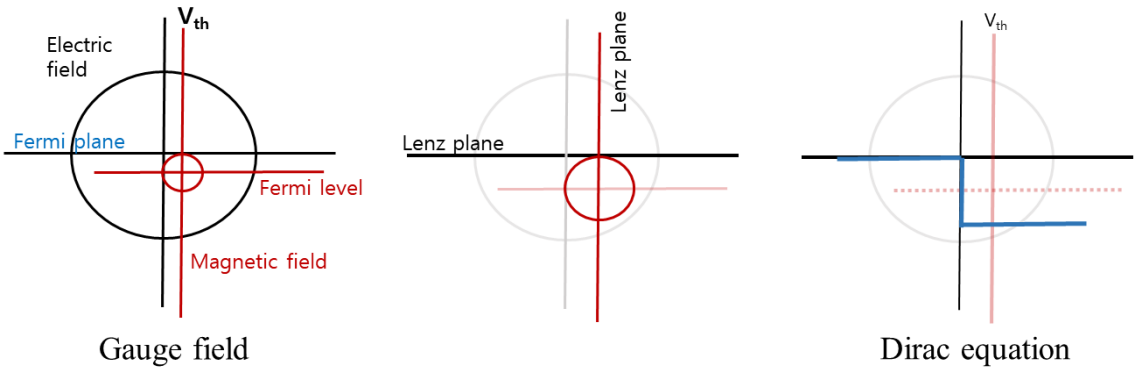

Fig. 1. Lenz's law for the electromagnetic energy conservation and lenz's plane for gauge field to separate matters and antimatters.

Matters and antimatters have electro-magnetic energy composed of electric field and magnetic field by electron matters and spin antimatters. In figure 1, matters are three-dimensional structures, and the antimatters are obtained from two-dimensional structures. The study of matters and antimatters has developed into classical mechanics that study matter and quantum mechanics that study the state of matter. The energy conservation law is maintained because it has the same energy value although the three dimensional kinetic energy ($E=mc^2$) and two dimensional wave energy ($E=h\gamma$). As the dimension changes, the plane of symmetry changes. In accordance with the Lenz Act, which is the energy conservation law of the electric field and the magnetic field, the Lenz plane, which becomes the reference plane where the electric field and the magnetic energy are

symmetrical, is the threshold voltage in three dimensions. It is Weyl fermion that the energy moves in one direction according to the threshold voltage. Dirac fermion and Majorana fermion are energy state that follow the Dirac function, which are treated in two-dimensional quantum mechanics. The two-dimensional Dirac function is symmetrical, and the criterion of symmetry is Fermi-level. Electrically, if the fermi-level and the Lenz plane are in the same position, the energy is in the Majorana fermion state. However, it is difficult to make in the case of Majorana fermion, and most of the energy is in the state of Dirac fermion or Weyl fermion.

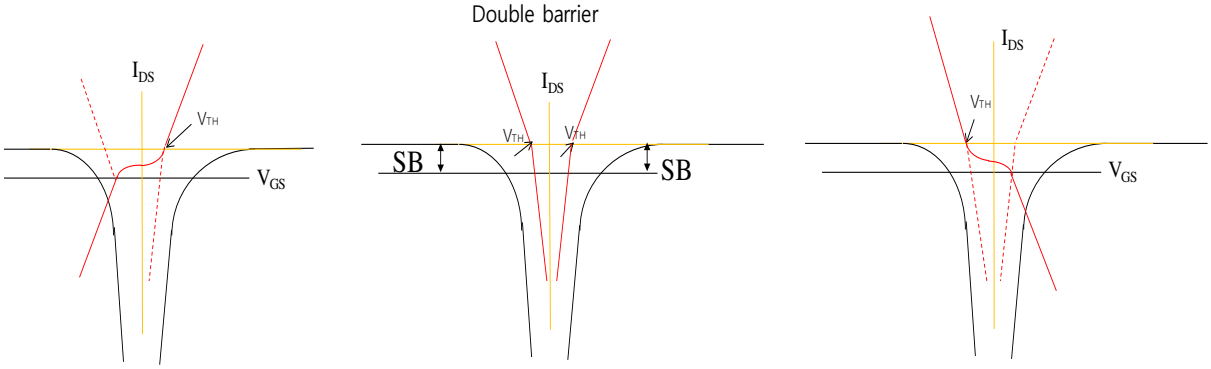

Fig. 2. Formation of depletion layer by double junction at schottky contact.

The depletion layer is caused by two PN junctions, and the depletion layer creates a schottky contact. As shown in figure 2, the schottky contact is caused by magnetic field energy generated by the potential barrier. The spin produced by magnetic energy moves in positive (+) direction current and negative (-) direction, resulting in spin current by rotation and divergence. Therefore, the spin current depends on the schottky contact. There is a Dirac fermion where the spin current in a double junction becomes stronger due to the occurrence of the gauge field, a Weyl fermion that weakens the spin current, and a Majorana fermion that does not have a schottky contact before the gauge field occurs. Since Majorana fermion, Dirac fermion, and Weyl fermion are spin currents, quantum spins hall effects and quantum tunneling phenomena by the antimatter are shown.

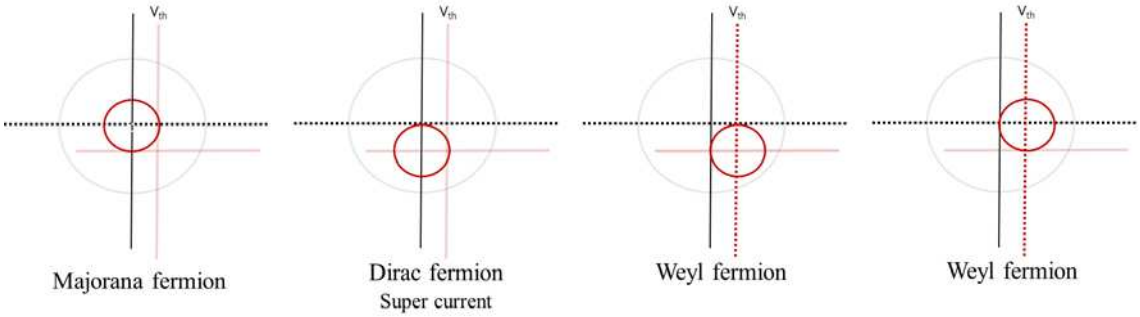

Fig. 3. Majorana fermion, Dirac fermion and Weyl fermion in according to the generation of gauge field.

Figure 3 shows the relationship between the occurrence of the gauge field in the general electric field and Majorana fermion and Dirac fermion and Weyl fermion. It explains the difference between Dirac fermion and Mayorana fermion, which operate on magnetic energy in negative current area. If the general electromagnetic field and the gauge field are matched, it becomes a Majorana fermion, and if it is inconsistent, it becomes a Dirac fermion or a Weyl fermion. Therefore, the Majorana fermion has both matters and antimatters. Weyl fermion also has both particles and carriers, but has high resistance. But Majorana fermion has no resistance. Dirac fermion, which has only the antimatter, also has no resistance. There is a difference in the method and amplification of electron energy of Majorana fermion and Dirac fermion.

Figure 4 shows that energy moves symmetrically from the gauge plane when the electromagnetic energy is transferred from the gauge field. Dirac fermion increases energy as the spin current moves to the charge current by C symmetry conservation, but the Majorana fermion decreases energy because there is no plane of symmetry in which the spin current can shift to the charge current. Because of the resistance, Weyl fermion is mostly composed of charge currents and has no gauge field for C symmetry.

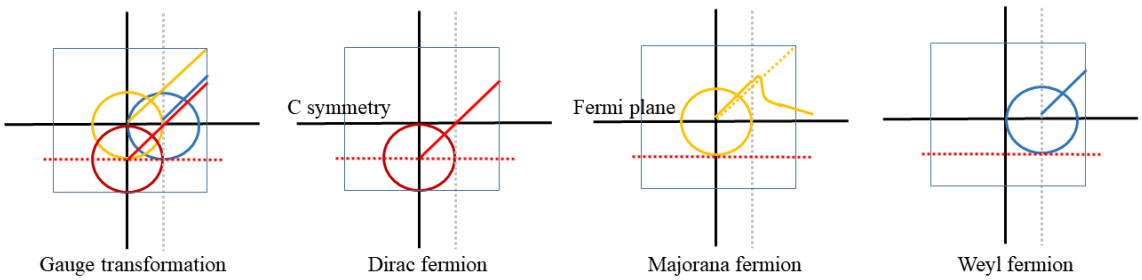

Fig. 4. Transfer characteristics of fermions and CP symmetry by electromagnetic energy transformation.

Current amplification of Dirac fermion is caused by quantum tunneling and C symmetry conservation.

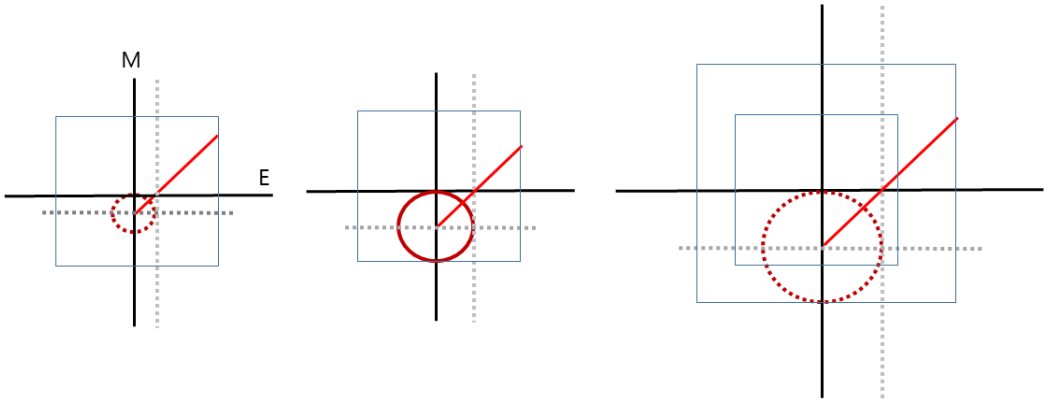

Fig. 5. Amplification of antimatters as Dirac fermion with quantum tunneling.

Thus, the Dirac fermion becomes the intermediate state of the CP symmetry conservation, the Majoran fermion is the CP symmetry vibration and the Weyl fermion is the middle state of the Dirac fermion and Majorana fermion.

3. Experimental method

The SiOC film was prepared by RF magnetron sputtering with a 2-in. diameter ceramic target (SiO:C, 97%:3% wt.) supplied by LTS Research Laboratories, Inc., U.S.A. The flow rate of the argon (99.9999%) was controlled by a mass flow controller (MFC) from 19~27 sccm for 20 min, and the sputtering RF power was 250W. The substrate temperature was kept constant at room temperature.

4. Results and discussions

(1) Quantum tunneling phenomenon with zero resistance

The I_{DS}-V_{GS} transfer characteristics of transistors were studied to identify the spin current characteristics of phase insulator. The SiOC (19 sccm) ~SiOC (27 sccm) transistor has shown bidirectional transfer characteristics as shown in figure 6. It is observed that the negative I_{DS} increases in SiOC (25 sccm). The logarithmic transformation was made as shown in figure 7 to identify quantum tunneling phenomena that occur when the resistance reaches zero. Tunneling is occurring at V_{DS} =0 V. As V_{DS} increases, tunneling is disappearing. When the internal magnetic field of phase insulator is large, tunneling phenomenon is caused by spin

current. The reason why it operates in both directions is because spin current flows.

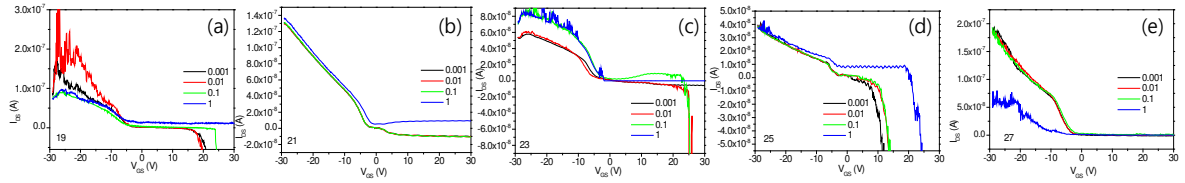

Fig. 6. Transfer characteristics of transistors in accordance with argon gas flow rates, (a) 19 sccm, (b) 21 sccm, (c) 23 sccm, (d) 25 sccm, (e) 27 sccm.

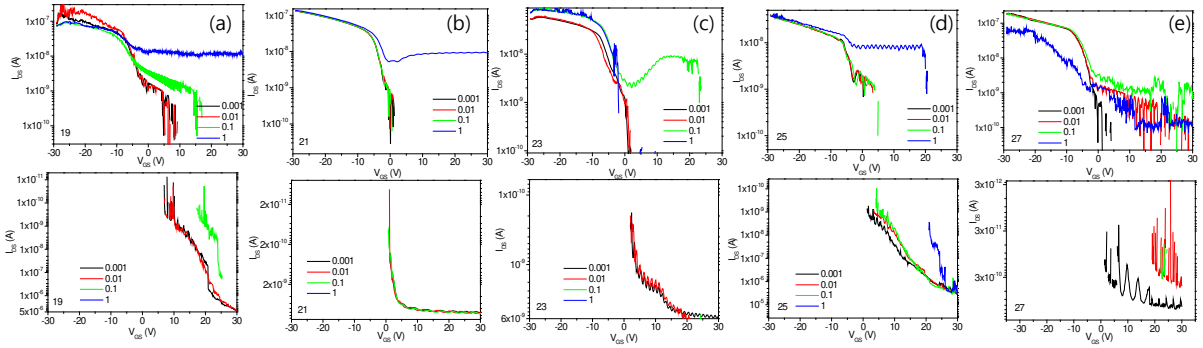

Fig. 7. Logarithm of transfer characteristics of transistors in accordance with argon gas flow rates, (a) 19 sccm, (b) 21 sccm, (c) 23 sccm, (d) 25 sccm, (e) 27 sccm.

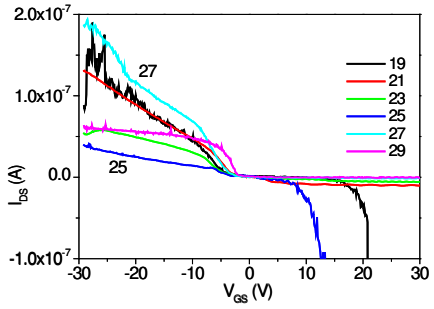

Figure 8. Comparison of I_{DS}-V_{GS} curves at V_{DS}=0.001 V to Again a symmetry by quantum tunneling pump phenomenon.

Figure 8 compares the I_{DS}-V_{GS} curve at V_{DS}=0.001 V. The lowest positive I_{DS} current and negative I_{DS} in the transistor of SiOC (25 sccm) are observed to increase the most. This is an advantageous condition for the transistors in SiOC (25 sccm) to have a quantum spin effect due to the relatively large amount of antimatters.

The I_{DS}-V_{DS} transmission characteristics of transistors were investigated as shown in the graph below in figure 9 to examine parity symmetry by the gauge field. The gauge field are made from a double junction in which the depletion layer is formed, as shown in figures 3 and 4.

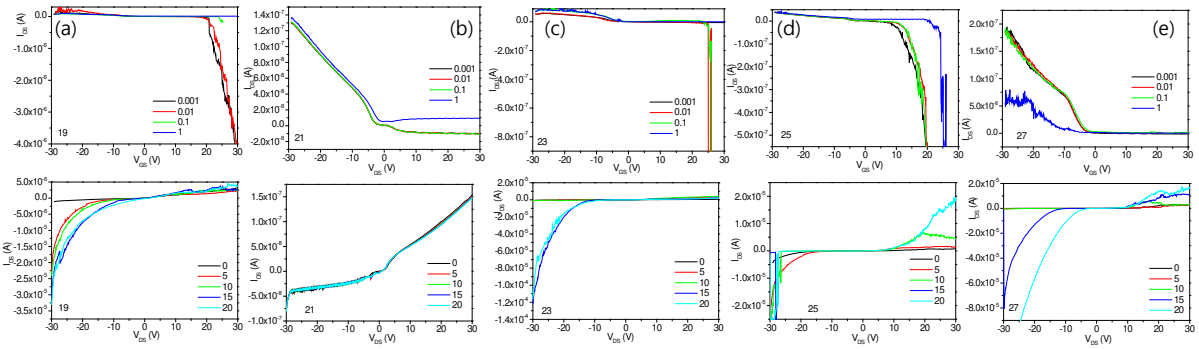

Fig. 9. I_{DS}-V_{DS} I/O characteristics of transistors and I_{DS}-V_{GS} transfer characteristics.

(2) P-symmetry violation of Majorana fermion with an ohmic contact and parity symmetry conservation of Dirac fermion due to the double junction

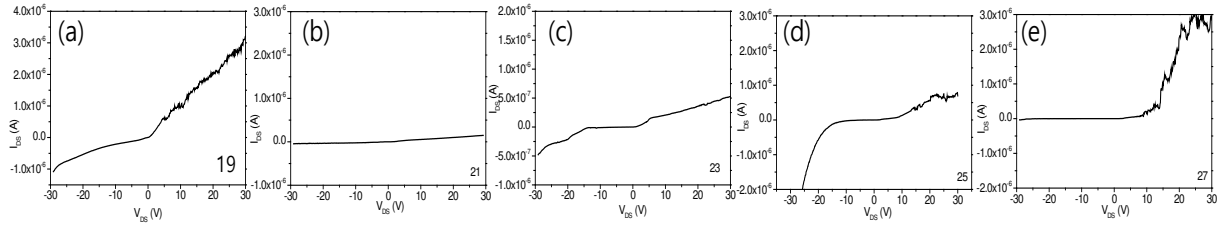

Fig. 10. I_{DS}-V_{DS} input/output characteristics of transistors; (a) 19 sccm; (b) 21 sccm; (c) 23 sccm; (d) 25 sccm; and (e) 27 sccm.

As shown in figure 10, 19 sccm and 27 sccm showed a significant increase in the positive I_{DS} current values. 25 sccm has a significant increase in the negative I_{DS} current value. In the junction characteristics in figure 11, the schottky junction was well done at 23 sccm and 25 sccm. Majorana fermion and Dirac fermion can be seen that the junction of schottky contact is important.

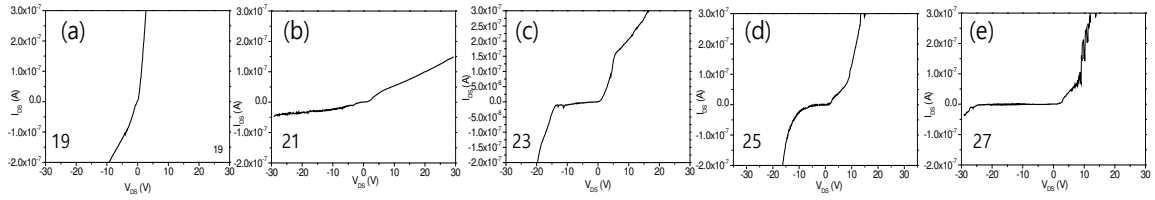

Fig. 11. Single schottky junction and double schottky junction according to contact properties at interfaces, (a) 19 sccm, (b) 21 sccm, (c) 23 sccm, (d) 25 sccm, and (e) 27 sccm.

I_{DS} current was compared from I_{DS}-V_{DS} input/output characteristics at V_{DS}=0V.

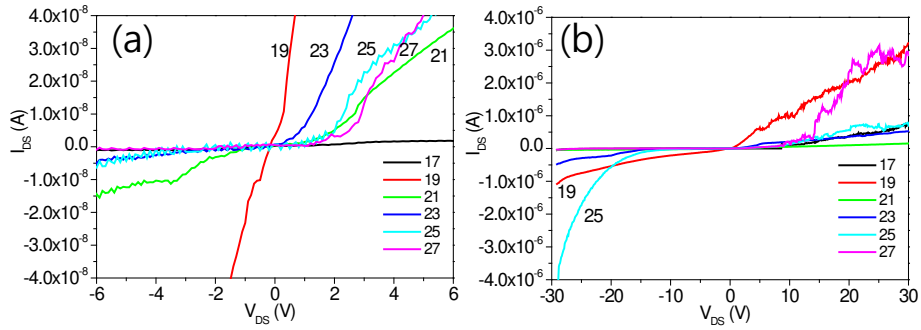

Fig. 12. Comparison of I_{DS}-V_{DS} transfer characteristics of transistors, (a) range of -4x10^{-8}<voltage<+4x10^{-8}, (b) range of -4x10^{-6}<voltage<+4x10^{-6}.

Comparing the I_{DS}-V_{DS} transmission characteristics of transistors in figure 12(a), large currents are dimmed at 19 sccm in areas where the voltage is low, but in figure 12(b), more current flows at 25 sccm as the voltage increases.
Figure 11 to 19sccm shows the ohmic contact and 25sccm shows the double junction characteristics. It can be seen that the current has increased at 25 sccm, where the spin current is strongly made. The spin current was not made because the schottky contact was not made at 19sccm. Therefore, 19sccm is Majorana fermion, and 25sccm is Dirac fermion.

(3) Symmetry conservation

Figure 13 shows the I_{DS}-V_{GS} transmission characteristics of quantum tunneling transistors at V_{DS}=0.001 V.

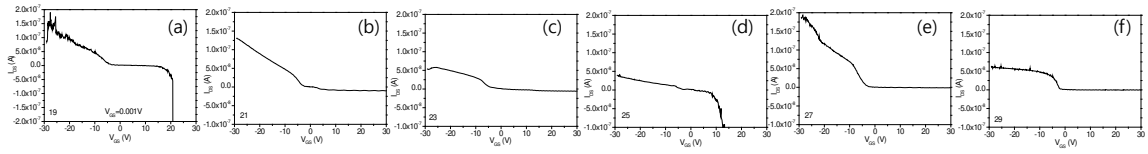

Fig. 13. I_{DS}-V_{GS} transfer characteristics of transistors at V_{DS}=0.001 V, (a) 19 sccm, (b) 21 sccm, (c) 23 sccm, (d) 25 sccm, (e) 27 sccm, (f) 29 sccm.

Parity symmetry overlaps figures 11 and figures 13 to examine symmetry.

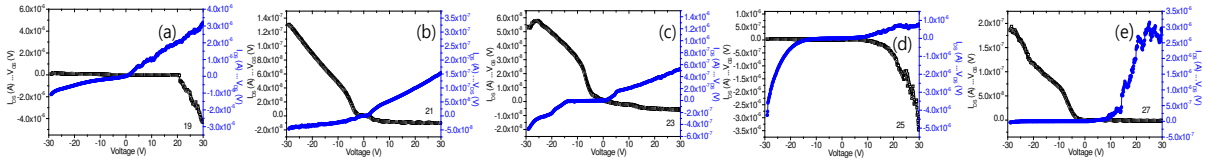

Figure 14. Comparison of symmetry between I_{DS}-V_{GS} curve and I_{DS}-V_{DS} curve, (a) 19 sccm, (b) 21 sccm, (c) 23 sccm, (d) 25 sccm, (e) 27 sccm, (f) 29 sccm.

Symmetry was shown at 25sccm, and as shown in Figure 14 (d), the Dirac fermion shows an increase in negative I_{DS} current. The 19 sccm without symmetry can be seen as a Majorana fermion by the symmetry breaking as shown in Figure 14(a). Figures 14(b), 14(c) and 14(e) show the intermediate characteristics of Dirac fermion and Majorana fermion, so they are Weyl fermion.

Figure 15 shows the results of parity symmetry on an electromagnetic plane.

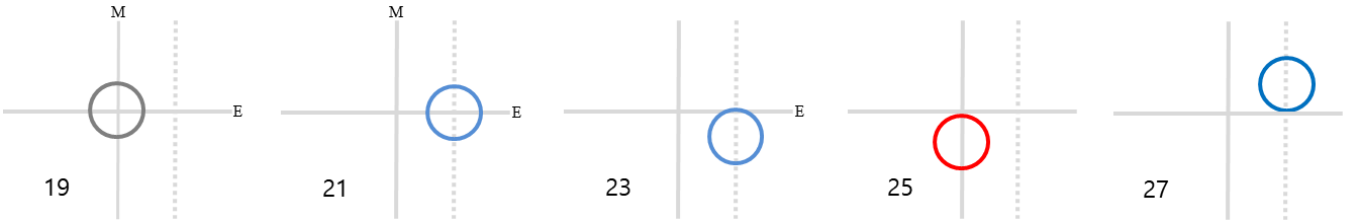

Fig. 15. The relationship between the electromagnetic plane and the fermion.

(4) Charge symmetry conservation for super currents

Dirac fermion has only spin current. Therefore, the spin current is caused by the super current because the symmetry conservation. The spin current that occurs when the resistance is zero is most magnetic energy, so it becomes a super current as energy is converted into charge current by C symmetry conservation.

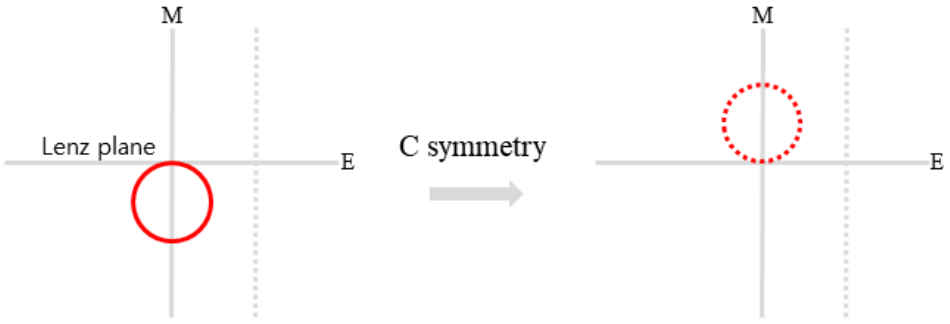

Fig. 16. Generation of super currents from spin currents to charge currents by C symmetry.

As shown in figure 16, the Dirac fermion is amplified by CP symmetry preservation. Current-voltage was measured with diode characteristics to examine the amplification effect of energy. Comparing the current voltage diode characteristics in figure 17, there is a lot of charge current flowing at 25 sccm. In figure 18, the current voltage diode characteristics show that the current is rapidly changing at 17 sccm and 29 sccm. The thin film of 19 sccm to 25 sccm shows the properties of phase insulator as negative current is increasing. Fermion is made by phase isolator, and it can be seen that it is a negative current.

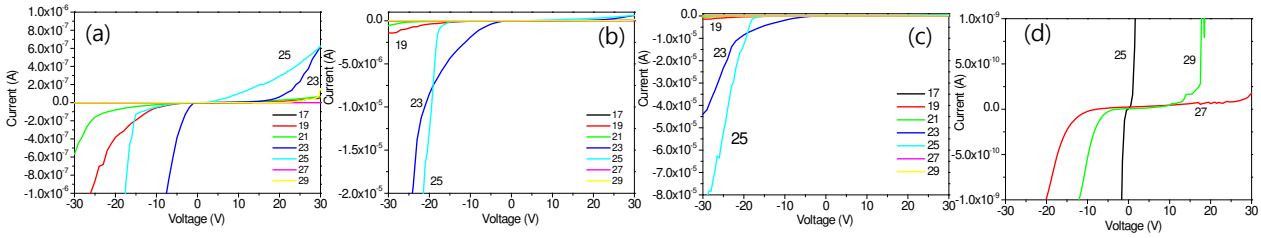

Fig. 17. Current-voltage properties of two port device as a diode.

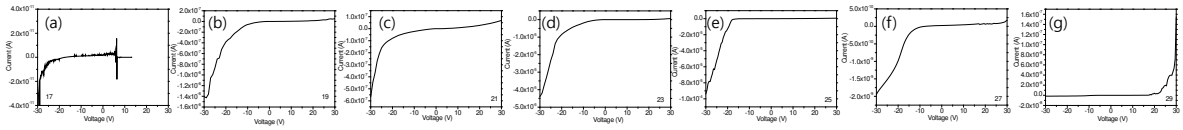

Fig. 18. Characteristic of currents, (a) 17 sccm, (b) 19 sccm, (c) 21 sccm, (d) 23 sccm, (e) 25 sccm, (f) 27 sccm, (g) 29 sccm.

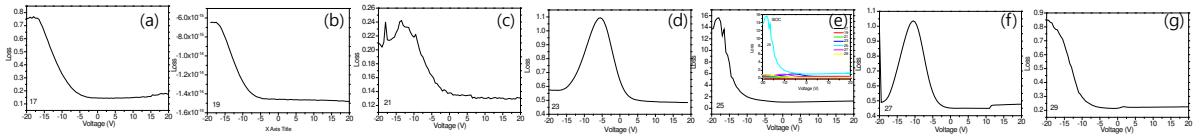

Fig. 19. Comparison of Loss, (a) 17 sccm, (b) 19 sccm, (c) 21 sccm, (d) 23 sccm, (e) 25 sccm, (f) 27 sccm, (g) 29 sccm.

Comparing the loss of the phase insulator SiOC thin film, the loss is rapidly increasing if the voltage is very low at 25 sccm as shown in figure 19. In figures 20(a) and 20(c), the capacitance is the largest at 25 sccm. And in figures 20(b) and 20(d), the 25 sccm loss is the largest. 19 sccm had the lowest capacitance and no loss.

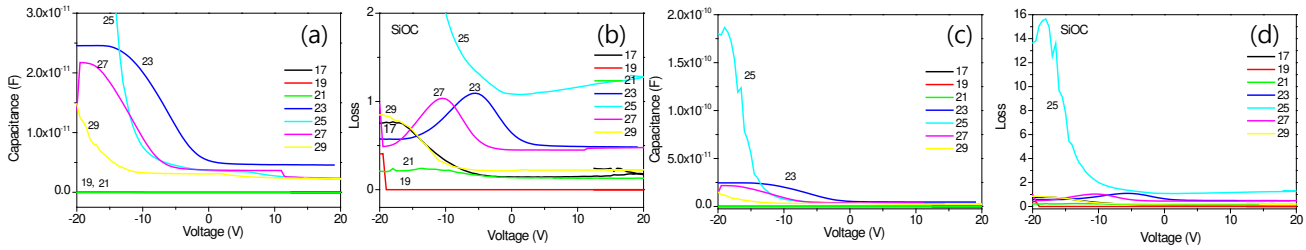

Fig. 20. Comparison of capacitance and loss as electrical properties of phase insulators, (a) capacitance in low areas, (b) loss in low areas, (c) capacitance in high areas, and (d) loss in high areas.

The phase isolator of 25 sccm has a large capacitance and a large loss at the same time. This is because the phase insulator has magnetic energy and negative resistance. Thus, the phase insulator of 25 sccm has a large loss, but the magnetic energy is so great that the capacitance is high that the current is greatly increased as shown in figure 17. Figure 7 shows that the I_{DS} current of 25 sccm is small, but as explained in figure 5, the current of 25 sccm is greatly increased due to the amplification effect of the antimatter, as shown in figure 17.

5. Conclusion

The double-schottky junction was made for the conservation of parity symmetry, and supercurrents were created by magnetic energy with strong Dirac fermion in narrow double-junctions. But the single schottky contacted Weyl fermion was not made of super current. Mjyorana fermion had the lowest capacitance and no loss, and no schottky junctions were made and ohmic contacts were made. Thus, symmetry violation was identified in Majorana fermion, and the current was relatively very low as the voltage increased. Parity symmetry conservation was confirmed from the electrical properties of transistors, and charge symmetry conservation was confirmed in diode properties.

References

1. Yoshishige Suzuki, Hitoshi Kubota, Spin-Torque Diode Effect and Its Application. *J Phys Soc Jpn***. 77,** 031002 (2008).

2. Philip F Bagwell. Suppression of the Josephson current through a narrow, mesoscopic, semicondu ctor channel by a single impurity. *Phys Rev B*, **46**, 12573-86 (1992).

3. Wei Han, YoshiChika Otani and Sadamichi Maekawa, Quantum materials for spin and charge conversion, *npj Quantum Materials*, **27**, 8308 (2018)。

4. Giant Transition-State Quasiparticle Spin-Hall Effect in an Exchange-Spin-Split Superconductor Detected by Nonlocal Magnon Spin Transport, Kun-Rok Jeon, Jae-Chun Jeon, Xilin Zhou, Andrea Migliorini, Jiho Yoon, and Stuart S. P. Parkin, *ACS Nano*, ***19***, 139– 152 (2020).

5. Wei Han, Sadamichi Maekawa and Xin-Cheng Xie, Spin current as a probe of quantum materials, *Nature Materials*, **19**, 139–152 (2020).

6. Oh T. Analysis of Surface Current by Quantum Tunneling Effect of Thin Film Transistors with Topological Insulators, *Scientific Reports*, **10** 9509 (2020).

7. Rui Wang, Onur Erten, Baigeng Wang, D.Y. Xing, Prediction of a topological p + ip excitonic insulator with parity anomaly. *Nature Communications*, **10**, 210 (2019).

8. Oh T. and Choi C. K., Comparison between SiOC Thin Films Fabricated by Using Plasma Enhance Chemical Vapor Deposition and SiO_2 Thin Films by Using Fourier Transform Infrared Spectroscopy. *J. Korean Phys. Soc.* **56,** 1150-1155 (2010).

9. Charles L. Kane, An insulator with a twist nature physics, *CONDENSED MATTER*, **4**, 348-349(2008).

10. Eric G Barbagiovanni, David J Lockwood Peter J Simpson, Lyudmila V Goncharova. Quantum confinement in Si and Ge nanostructures: Theory and experiment. *Appl Phys Rev*. **1** 011302 (2014).

11. T Edvinsson. Optical quantum confinement and photocatalytic properties in two-, one- and zero-dimensional nanostructures. *Royal society open science*, **5**, 180387 (2018).

12. J Frenkel. On pre-breakdown phenomena in insulators and electronic semi-conductors. *Phys Rev.* **54,** 647–648 (1938).

13. Yuan Li, Yong Sun, Weiwei Zhu, Zhiwei Guo, Jun Jiang, Toshikaze Kariyado, Hong Che and Xiao Hu, Topological LC-circuits based on microstrips and observation of electromagnetic modes with orbital angular momentum, *Nature Communications*, **9**, 4598 (2018).

14. Jungho Mun, Minkyung Kim, Younghwan Yang, Trevon Badloe, Jincheng Ni, Yang Chen, Cheng-Wei Qiu and Junsuk Rho, Mun et al. Electromagnetic chirality: from fundamentals to nontraditional chiroptical phenomena, *Light: Science & Applications,* **9**, 139 (2020).

15. P B Wiegmann. One-dimensional Fermi system and plane xy model. *J Phys C Solid State Phys.* **11**, 1583 (1978).

16. Raymond T Tung. The physics and chemistry of the Schottky barrier height. *Appl Phys Rev.* **1,** 011304(2014).

17. J Maserjian, N Zamani. Behavior of the Si/SiO_2 interface observed by Fowler Nordheim tunneling . *Appl Phys Lett.* **53**, 559–567 (1982).

18. Jeffrey C K, et al. Evidence of ultra-low-k dielectric material degradation and nanostructure alteration of the Cu/ultra-low-k interconnects in time-dependent dielectric breakdown failure. *Appl Phys Lett*. **102**, 022908 (2013).

19. J. G. Simmon. Poole-Frenkel Effect and Schottky Effect in Metal-Insulator-Metal Systems. *Phys Rev.* **155**, 657–660 (1967).

20. L L Chang, L Esaki, R Tsu. Resonant tunneling in semiconductor double barriers. *Appl Phys Lett.* **24**, 593-595 (1974)

21. Harold P Hjalmarson, P Vogl, D J Wolford, John D Dow. Theory of Substitutional Deep Traps i n Covalent Semiconductors. *Phys Rev Lett.* **44**, 810-813 (1980).

22. Oh T. Organic Thin-Film Transistors Using Pentacene and SiOC Film, *IEEE TRANSACTIONS ON NANOTECHNOLOGY,* **5(1),** 23, (2006)

23. Majorana zero modes and topological quantum computation, Sankar Das Sarma, Michael Freedman & Chetan Nayak, *npj Quantum Information* volume 1, Article number: 15001 (2015)

24. Dezheng Yang, Fangcong Wang, Yang Ren Yalu Zuo, Yong Peng, Shiming Zhou, Desheng Xue. A Large Magnetoresistance Effect in p–n Junction Devices by the Space-Charge Effect. *Adv Funct Mater*. **23,** 2918–2923 (2013).

25. M. S. Sodha, A. Dixit and S. Srivastava, *Applied Physics Letters*, **94**, 251501 (2009)

26. N V Volkov, A S Tarasov, E V Eremin, F A Baron, S N Varnakov, S G Ovchinnikov. Extremely large magnetoresistance induced by optical irradiation in the Fe/SiO_2/p-Si hybrid structure with Schottky barrier. *J Appl Phys*. **114**, 09 (2013)

Author contributions

Oh T. conceived the study. All authors designed the experiment(s), and analyzed the results. All authors discussed the results and contributed to writing the manuscript.

Competing interests. All other authors have no conflict of interest to declare.

Figure captions

Fig. 1. Lenz's law for the electromagnetic energy conservation and lenz's plane for gauge field to separate matters and antimatters.

Fig. 2. Formation of depletion layer by double junction at schottky contact.

Fig. 3. Majorana fermion, Dirac fermion and Weyl fermion in according to the generation of gauge field.

Fig. 4. Transfer characteristics of fermions and CP symmetry by electromagnetic energy transformation.

Fig. 5. Amplification of antimatters as Dirac fermion with quantum tunneling.

Fig. 6. Transfer characteristics of transistors in accordance with argon gas flow rates, (a) 19 sccm, (b) 21 sccm, (c) 23 sccm, (d) 25 sccm, (e) 27 sccm.

Figure 8. Comparison of I_{DS}-V_{GS} curves at V_{DS}=0.001 V to Again a symmetry by quantum tunneling pump phenomenon.

Fig. 9. I_{DS}-V_{DS} I/O characteristics of transistors and I_{DS}-V_{GS} transfer characteristics.

Fig. 10. I_{DS}-V_{DS} input/output characteristics of transistors; (a) 19 sccm; (b) 21 sccm; (c) 23 sccm; (d) 25 sccm; and (e) 27 sccm.

Fig. 11. Single schottky junction and double schottky junction according to contact properties at interfaces, (a) 19 sccm, (b) 21 sccm, (c) 23 sccm, (d) 25 sccm, and (e) 27 sccm.

Fig. 12. Comparison of I_{DS}-V_{DS} transfer characteristics of transistors, (a) range of $-4x10^{-8}$<voltage<$+4x10^{-8}$, (b) range of $-4x10^{-6}$<voltage<$+4x10^{-6}$.

Fig. 13. I_{DS}-V_{GS} transfer characteristics of transistors at V_{DS}=0.001 V, (a) 19 sccm, (b) 21 sccm, (c) 23 sccm, (d) 25 sccm, (e) 27 sccm, (f) 29 sccm.

Figure 14. Comparison of symmetry between I_{DS}-V_{GS} curve and I_{DS}-V_{DS} curve, (a) 19 sccm, (b) 21 sccm, (c) 23 sccm, (d) 25 sccm, (e) 27 sccm, (f) 29 sccm.

Fig. 15. The relationship between the electromagnetic plane and the fermion.

Fig. 16. Generation of super currents from spin currents to charge currents by C symmetry.

Fig. 17. Current-voltage properties of two port device as a diode.

Fig. 18. Characteristic of currents, (a) 17 sccm, (b) 19 sccm, (c) 21 sccm, (d) 23 sccm, (e) 25 sccm, (f) 27 sccm, (g) 29 sccm.

Fig. 19. Comparison of Loss, (a) 17 sccm, (b) 19 sccm, (c) 21 sccm, (d) 23 sccm, (e) 25 sccm, (f) 27 sccm, (g) 29 sccm.

Fig. 20. Comparison of capacitance and loss as electrical properties of phase insulators, (a) capacitance in low areas, (b) loss in low areas, (c) capacitance in high areas, and (d) loss in high areas.

Figures

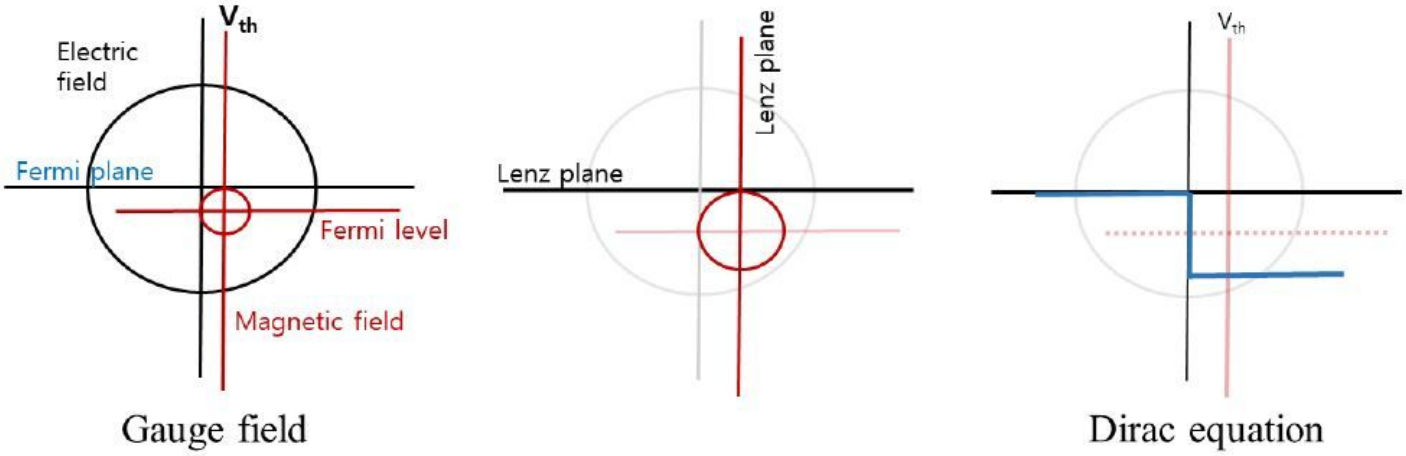

Figure 1

Lenz's law for the electromagnetic energy conservation and lenz's plane for gauge field to separate matters and antimatters.

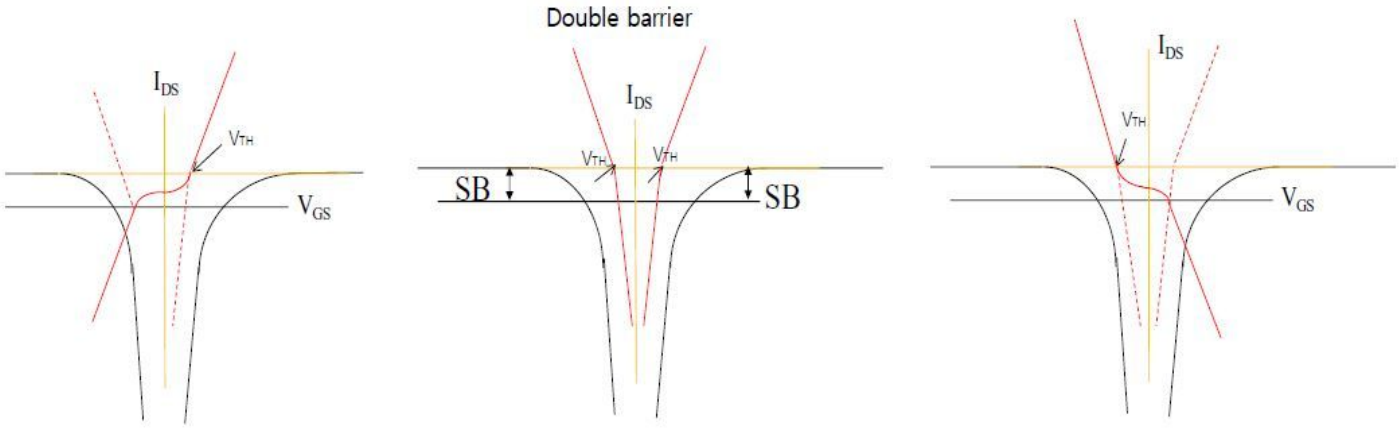

Figure 2

Formation of depletion layer by double junction at schottky contact.

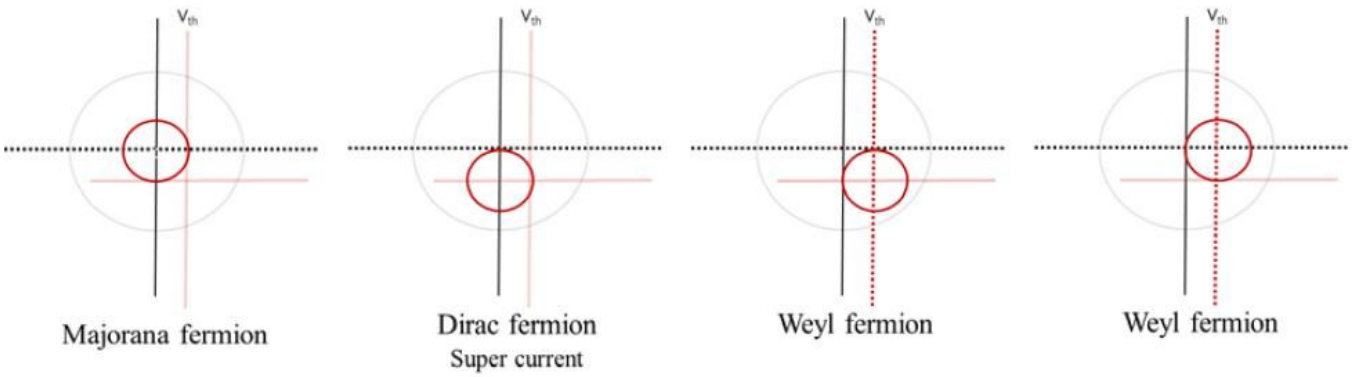

Figure 3

Majorana fermion, Dirac fermion and Weyl fermion in according to the generation of gauge field.

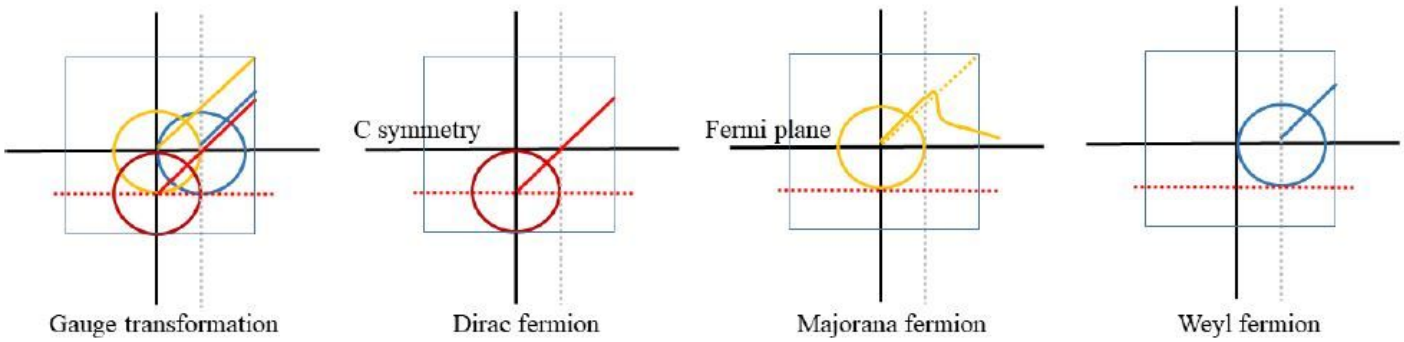

Figure 4

Transfer characteristics of fermions and CP symmetry by electromagnetic energy transformation.

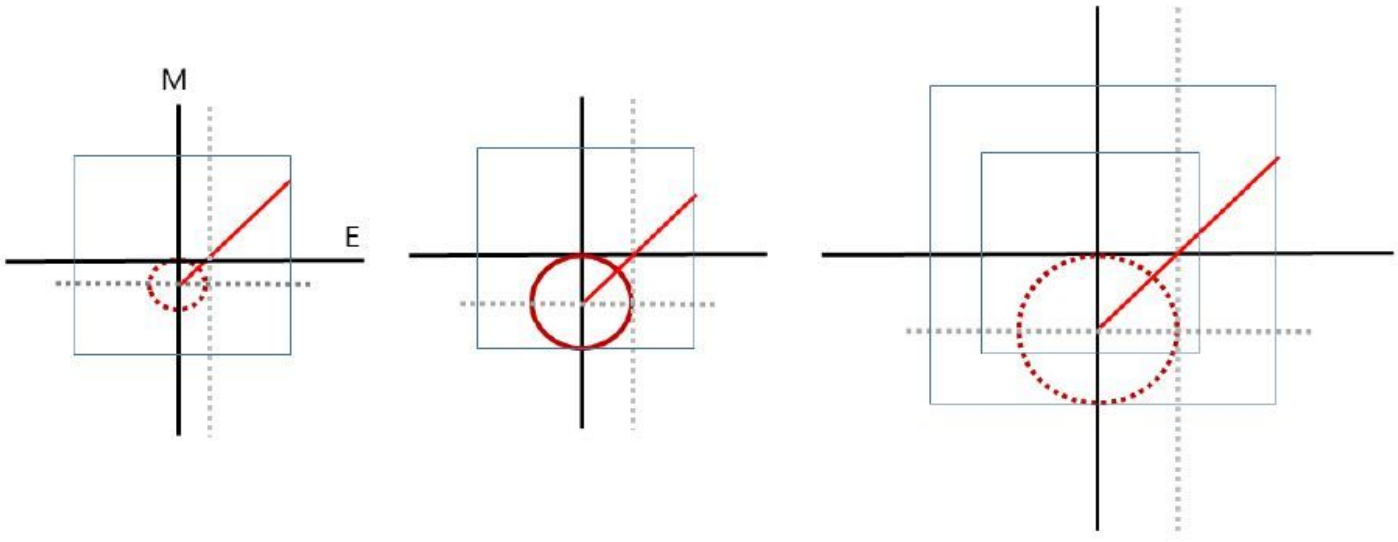

Figure 5

Amplification of antimatters as Dirac fermion with quantum tunneling.

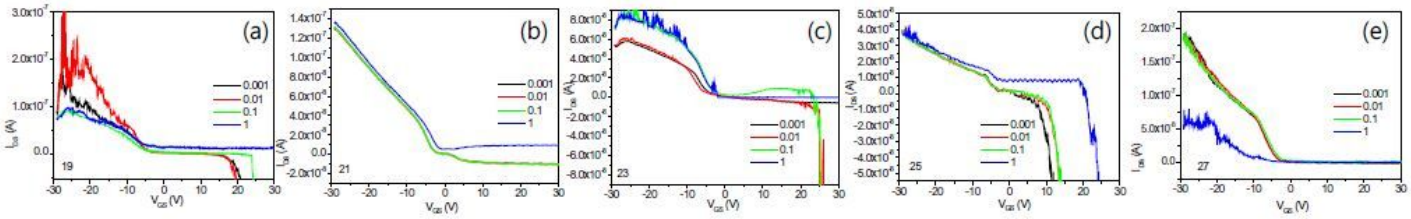

Figure 6

Transfer characteristics of transistors in accordance with argon gas flow rates, (a) 19 sccm, (b) 21 sccm, (c) 23 sccm, (d) 25 sccm, (e) 27 sccm.

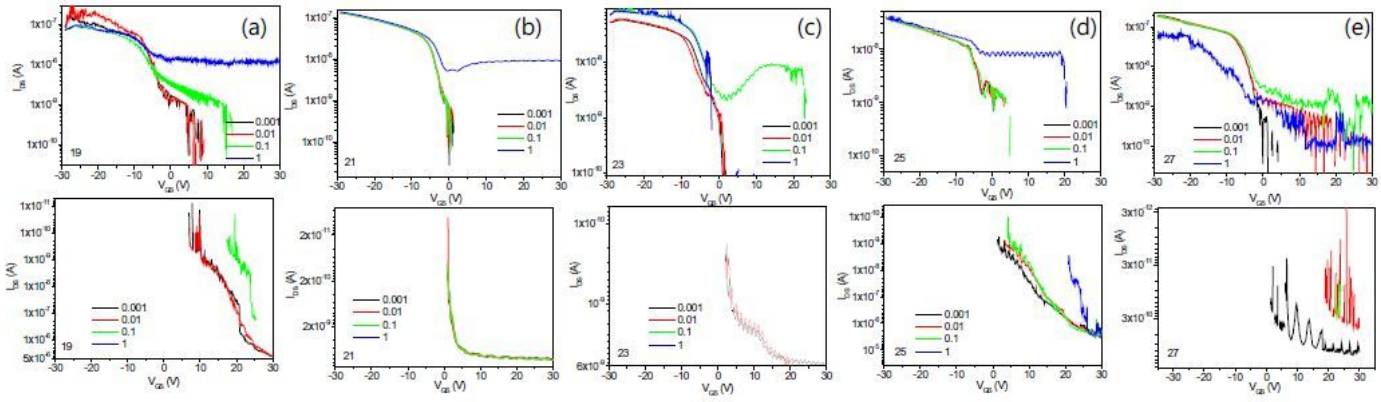

Figure 7

Logarithm of transfer characteristics of transistors in accordance with argon gas flow rates, (a) 19 sccm, (b) 21 sccm, (c) 23 sccm, (d) 25 sccm, (e) 27 sccm.

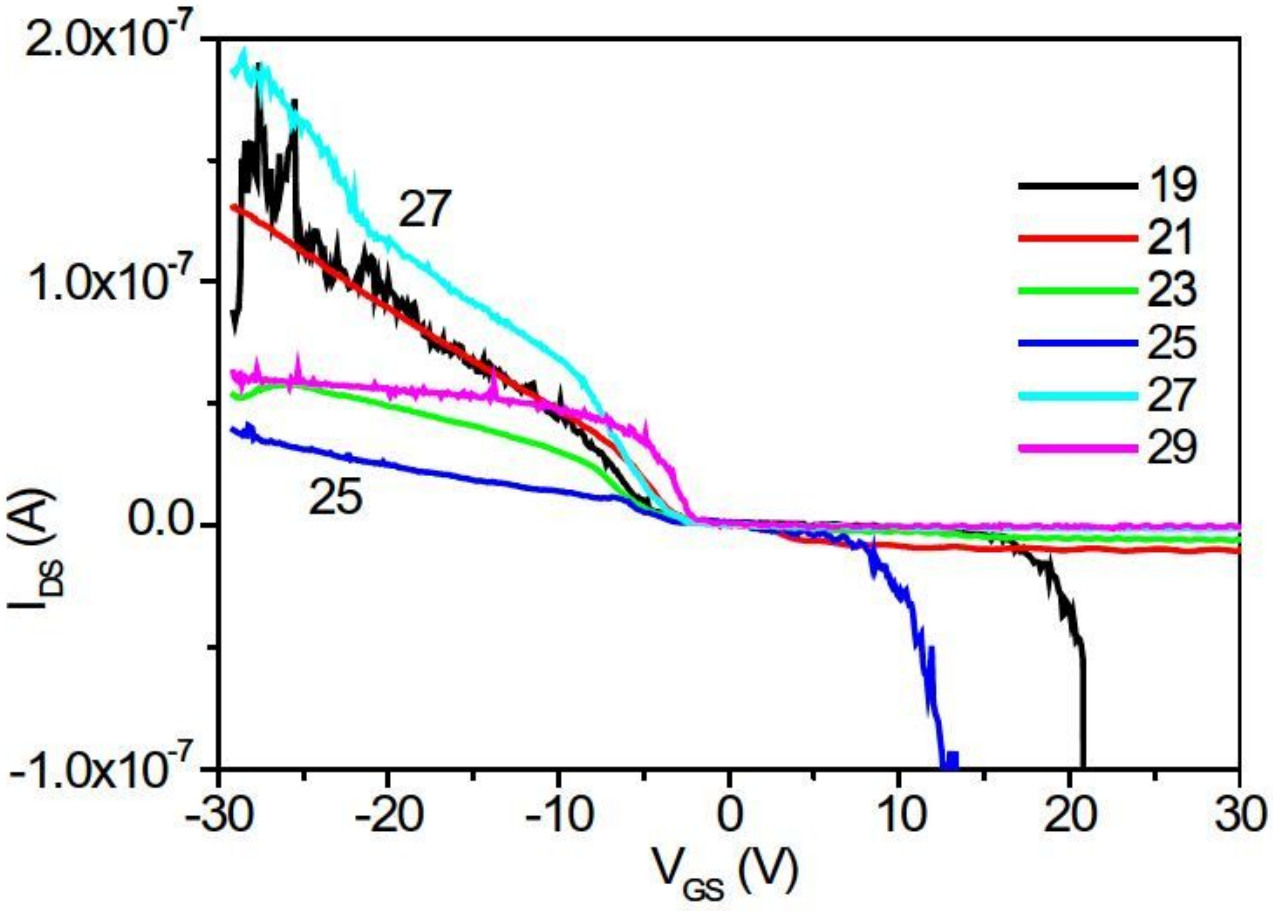

Figure 8

Comparison of IDS-VGS curves at VDS=0.001 V to Again a symmetry by quantum tunneling pump phenomenon.

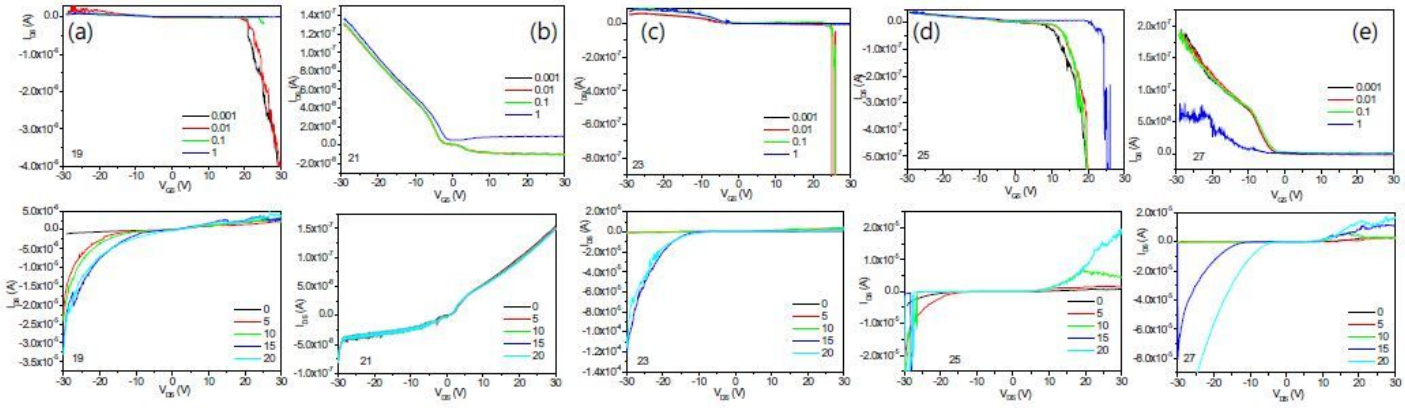

Figure 9

IDS-VDS I/O characteristics of transistors and IDS-VGS transfer characteristics.

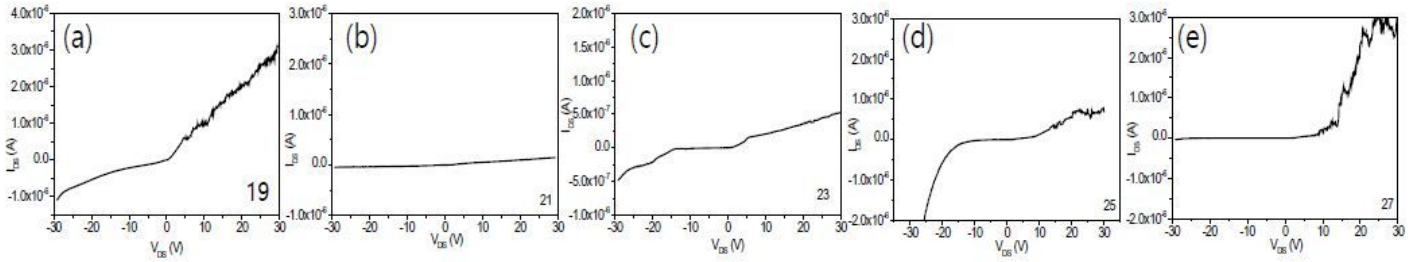

Figure 10

IDS-VDS input/output characteristics of transistors; (a) 19 sccm; (b) 21 sccm; (c) 23 sccm; (d) 25 sccm; and (e) 27 sccm.

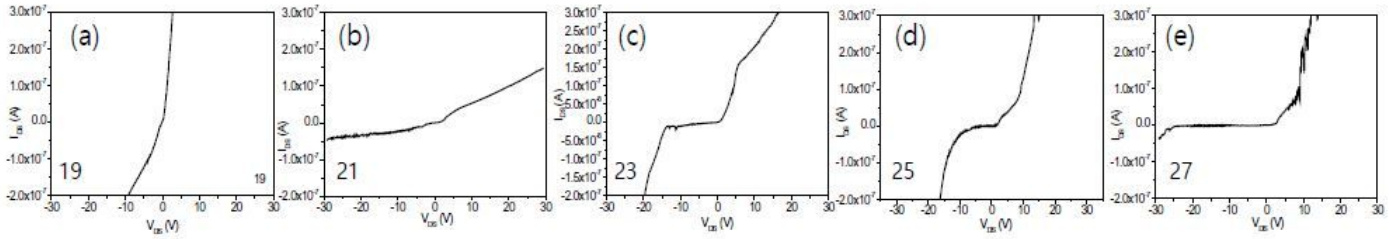

Figure 11

Single schottky junction and double schottky junction according to contact properties at interfaces, (a) 19 sccm, (b) 21 sccm, (c) 23 sccm, (d) 25 sccm, and (e) 27 sccm.

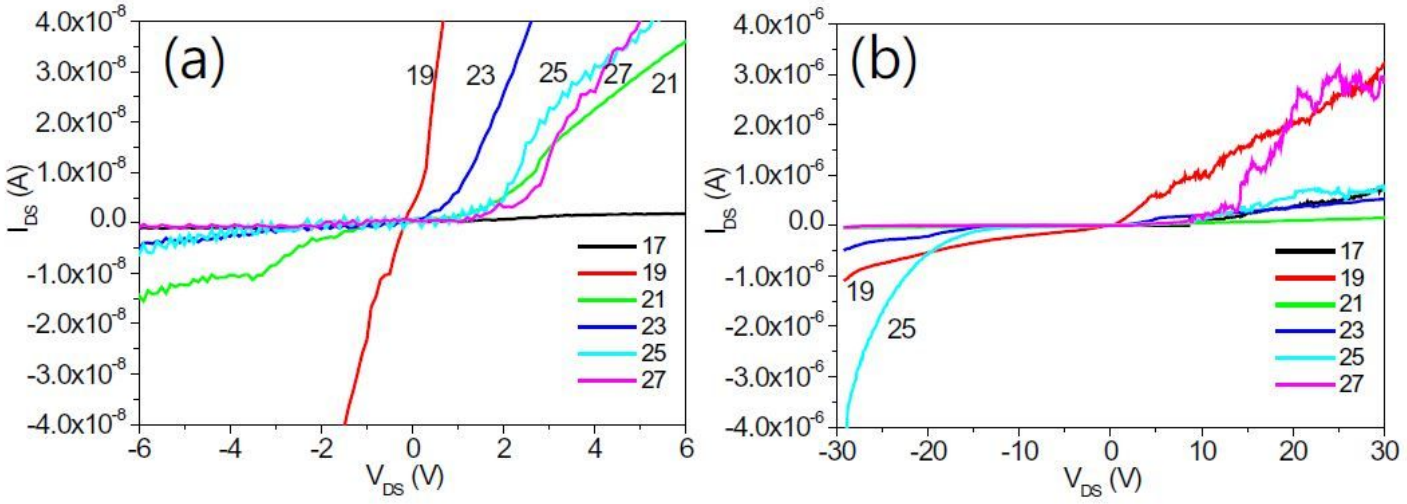

Figure 12

Comparison of IDS-VDS transfer characteristics of transistors, (a) range of -4x10-8<voltage<+4x10-8, (b) range of -4x10-6<voltage<+4x10-6.

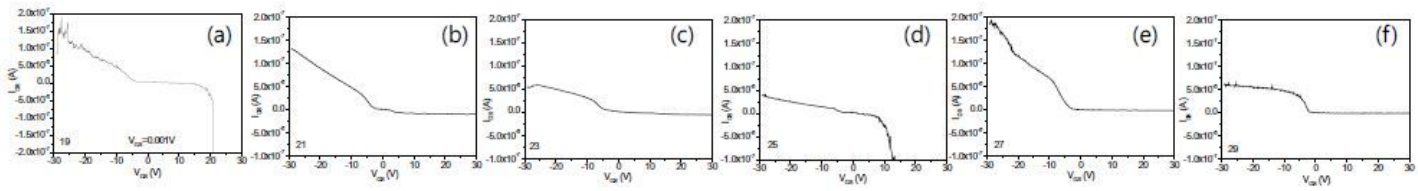

Figure 13

IDS-VGS transfer characteristics of transistors at VDS=0.001 V, (a) 19 sccm, (b) 21 sccm, (c) 23 sccm, (d) 25 sccm, (e) 27 sccm, (f) 29 sccm.

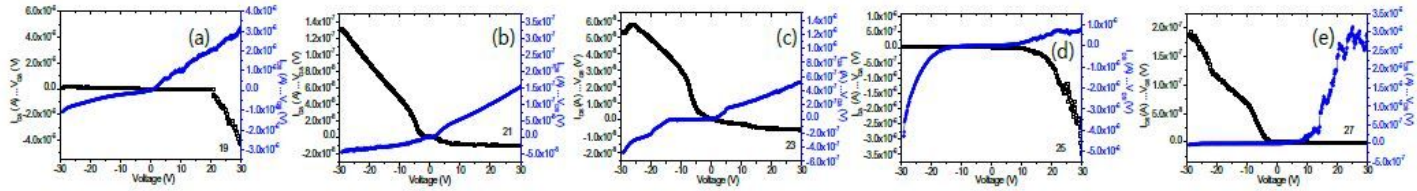

Figure 14

The relationship between the electromagnetic plane and the fermion.

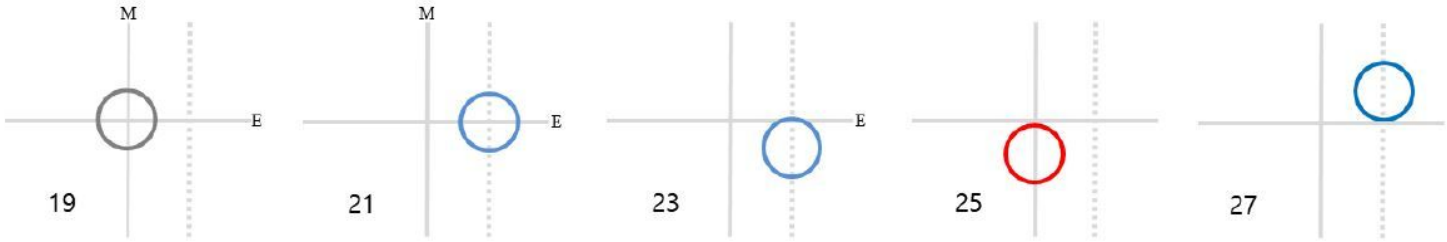

Figure 15

Generation of super currents from spin currents to charge currents by C symmetry.

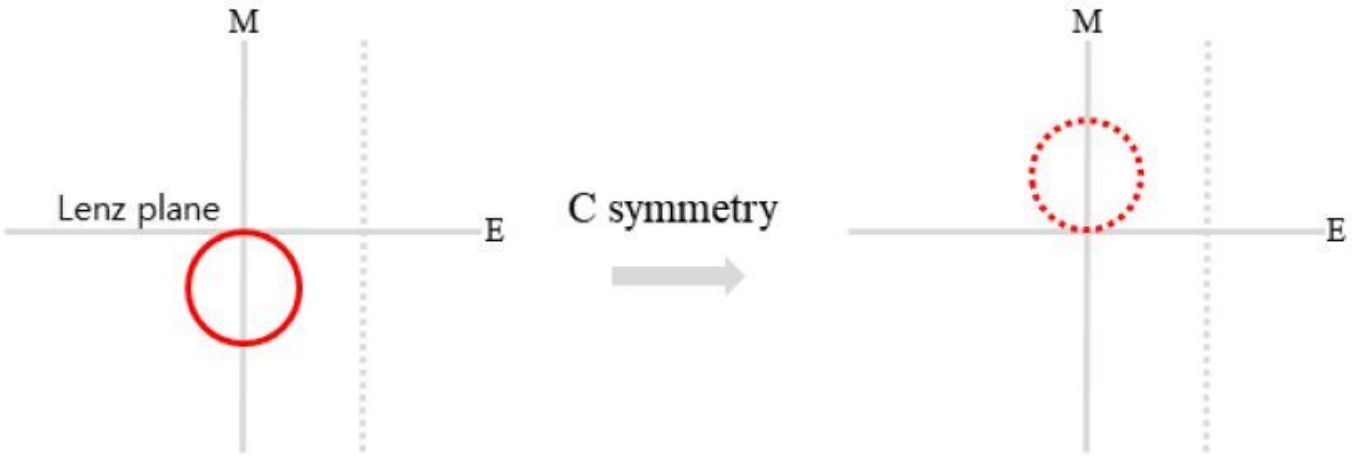

Figure 16

Current-voltage properties of two port device as a diode.

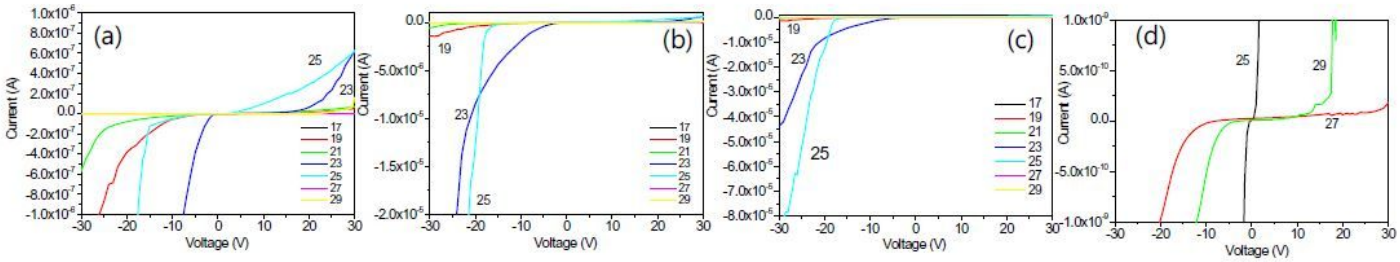

Figure 17

Current-voltage properties of two port device as a diode.

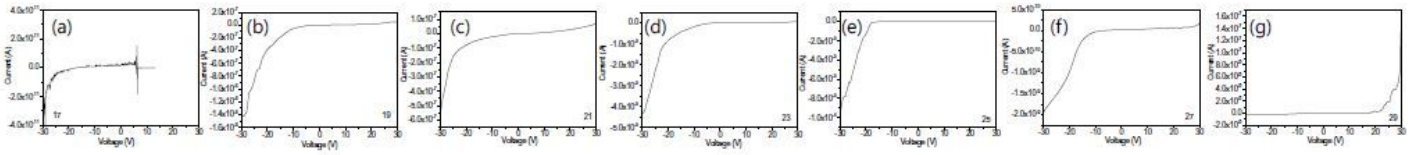

Figure 18

Characteristic of currents, (a) 17 sccm, (b) 19 sccm, (c) 21 sccm, (d) 23 sccm, (e) 25 sccm, (f) 27 sccm, (g) 29 sccm.

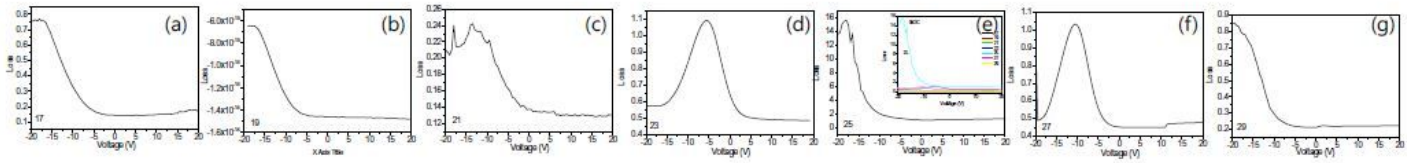

Figure 19

Comparison of Loss, (a) 17 sccm, (b) 19 sccm, (c) 21 sccm, (d) 23 sccm, (e) 25 sccm, (f) 27 sccm, (g) 29 sccm.

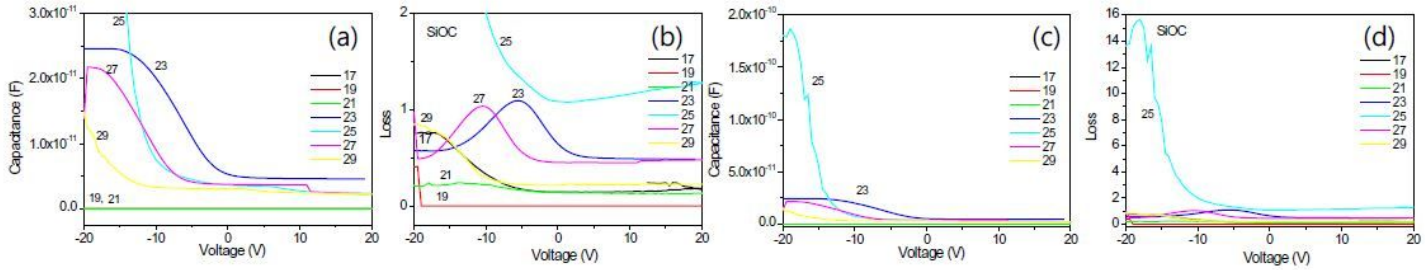

Figure 20

Comparison of capacitance and loss as electrical properties of phase insulators, (a) capacitance in low areas, (b) loss in low areas, (c) capacitance in high areas, and (d) loss in high areas.